Icarus 280 (2016) 255–267

Contents lists available at ScienceDirect

Icarus

journal homepage: www.elsevier.com/locate/icarus

Laboratory measurements of the 5–20 cm wavelength opacity of ammonia, water vapor, and methane under simulated conditions for the deep jovian atmosphere

Amadeo Bellotti[a,*], Paul G. Steffes[a], Garrett Chinsomboom[a,b]

[a] School of Electrical and Computer Engineering, Georgia Institute of Technology, Atlanta, GA 30332-0250, United States
[b] Abbott Medical Optics, 510 Cottonwood Dr., Milpitas, CA 95035, United States

ARTICLE INFO

Article history:
Received 8 April 2016
Revised 30 June 2016
Accepted 20 July 2016
Available online 29 July 2016

Keywords:
Jupiter, atmosphere
Radio observations
Atmospheres, composition
Spectroscopy
Experimental techniques

ABSTRACT

Over the past decade, several extensive laboratory studies have been conducted of the microwave opacity of ammonia and water vapor in preparation for interpretation of the precise measurements of jovian microwave emission to be made with the Microwave Radiometer (MWR) instrument aboard the NASA Juno Mission. (See, e.g., Hanley et al. [2009] Icarus, 202, 316–335; Karpowicz and Steffes [2011a] Icarus 212, 210–223; Karpowicz and Steffes [2011b] Icarus 214, 783; Devaraj et al. [2014] Icarus, 241, 165–179) These works included models for the opacity of these constituents valid over the pressure and temperature ranges measured in the laboratory experiments (temperatures up to 500 K and pressures up to 100 bars). However, studies of the microwave emission made using these models indicate that significant contributions to the emission at the 24-cm and 50-cm wavelengths to be measured by the Juno MWR will be made by layers of the atmosphere with temperatures at or exceeding 600 K. While the ammonia opacity models described by Hanley et al. (2009) and Devraj et al. (2014) give consistent results at temperatures up to 500 K (within 6%), they diverge significantly at temperatures and pressures exceeding 550 K and 50 bars, respectively. Similarly, at temperatures above 500 K, the model for water vapor opacity developed by Karpowicz and Steffes (2011a,b) exhibits non-physical attributes. To resolve these ambiguities, we have conducted laboratory measurements of the microwave opacity of ammonia at temperatures up to 600 K and that for water vapor at temperatures up to 600 K. Additionally, since the microwave opacity of ammonia is influenced by pressure-broadening from methane (a significant constituent in jovian atmospheres), measurements of the effects of methane on the ammonia absorption spectrum have also been conducted. These measurements have resulted in updated models for the opacities of ammonia and water vapor under conditions of the deep jovian atmosphere.

1. Introduction

Jupiter's microwave emission spectrum (both centimeter- and millimeter-wavelengths) consists of both thermal and non-thermal components. The thermal emission originates from the neutral atmosphere while the non-thermal is from the electrons and ions trapped in Jupiter's inner radiation belts. While ground-based radio observations at frequencies greater then 3 GHz (10 cm) are dominated by thermal emissions, at frequencies less then 3 GHz the non-thermal (synchrotron emissions) dominate (Berge and Gulkis, 1976; de Pater et al., 2003). Even at 10 GHz (3 cm) there is approximately a 10% contribution from the synchrotron component to the total emission from Jupiter (Berge and Gulkis, 1976; de Pater et al., 2003). The NASA Juno mission was launched in August 2011 with the goal to achieve 36 highly elliptical 14-day polar orbits, allowing atmospheric observations from low altitude, thus avoiding the synchrotron radiation (Matousek, 2005). From this vantage point, the microwave radiometer (MWR) onboard Juno will measure the thermal emissions from the atmosphere of Jupiter in the 0.6–22 GHz (50–1.36 cm) range using six separate channels (Pingree et al., 2008).

The primary goal of the Juno MWR is to measure the abundance of water and ammonia in the deep atmosphere of Jupiter. Studying the composition of Jupiter will aid in the studies of our planetary system's creation and evolution.

It is well known that the microwave emission spectrum of Jupiter's atmosphere reflects the abundance and distribution of constituents such as ammonia and water vapor (Janssen et al., 2005),

* Corresponding author.
E-mail address: bellotta@gatech.edu (A. Bellotti).

http://dx.doi.org/10.1016/j.icarus.2016.07.013
0019-1035/

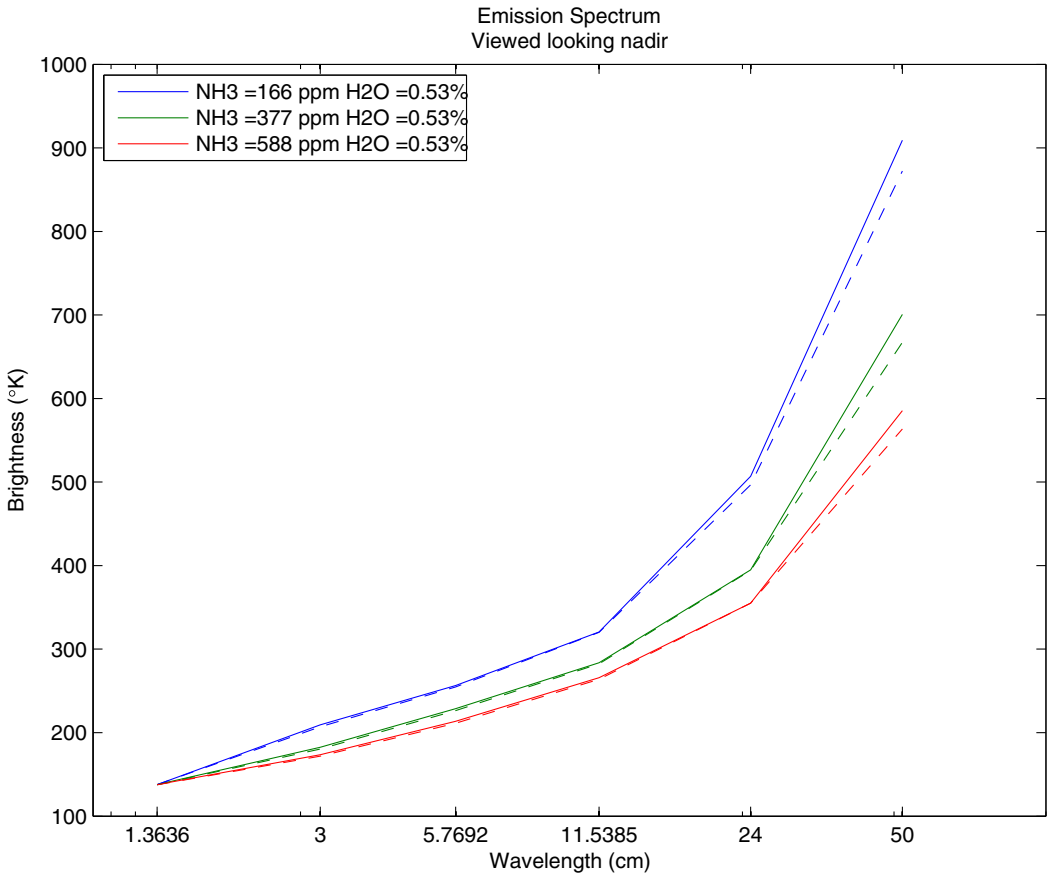

Fig. 1. The radiative transfer results with varying ammonia abundances. The solid line is the emission using the Hanley et al. (2009) model and the dashed is using the Devaraj et al. (2014) model.

but there are a number of factors that can limit the accuracy of using microwave remote sensing to measure these constituents (de Pater et al., 2005). The most important of these factors is the knowledge of the microwave absorption properties of these constituents under jovian conditions. These properties are dependent on the observation frequency and the temperature, pressure, and composition (fTPC space) of the atmosphere (Janssen, 1993). To interpret the observed emission spectra of the jovian atmospheres, the emission spectra are compared with accurate jovian atmospheric models and consistent physical profiles of various constituents are obtained. While a lack of laboratory measurements of the centimeter- and millimeter-wavelength properties of various gases has been cited as a major hindrance for modeling the atmosphere (de Pater et al., 2005; de Pater and Mitchell, 1993), recent measurement campaigns (Devaraj et al., 2014; Hanley et al., 2009; Karpowicz and Steffes, 2011a,b) have made great strides in better understanding these properties.

The atmosphere of Jupiter and other jovian planets (Saturn, Uranus, and Neptune) is primarily composed of hydrogen (H_2) and helium (He), with various trace constituents such as ammonia (NH_3), water vapor (H_2O), methane (CH_4), hydrogen sulfide (H_2S), and phosphine (PH_3) (Atreya et al., 2003; de Pater and Lissauer, 2001). In Jupiter's atmosphere, gaseous ammonia is the strongest contributor to the absorption at centimeter-wavelengths. Hence, accurate laboratory measurements of the microwave opacity of ammonia facilitate accurate retrievals of the concentration and distribution of ammonia as well as that of water vapor by the Juno MWR.

Studies of the microwave emission using JPL's Juno Atmosphere Model and Radiative Transfer Code (JAMRT, described in Janssen et al., 2013) indicates a significant contribution of the emission at 24 and 50 cm wavelengths to the retrieval of the ammonia and water vapor distribution in Jupiter's atmosphere. These wavelengths have been shown to originate from deep within the jovian atmospheres (with temperatures at or exceeding 600 K). Since the absorption models created for ammonia and water vapor have been based on laboratory measurements reaching only 500 K, it is important to carefully evaluate any extrapolation of these two absorption models to higher temperatures.

1.1. Ammonia

The motivation behind this work is the difference in the calculated microwave emission from the jovian atmosphere when the absorption model for ammonia is changed between the Devaraj et al. (2014) model and the Hanley et al. (2009) model. These two models perform equally well when compared to laboratory data relevant to Jupiter (frequencies under 27 GHz) (Devaraj et al., 2014). While the models are similar in the measured fTPC space, they differ significantly when extrapolated to higher temperatures. The differences between the two models significantly change the modeled emission at 600 MHz as modeled using JAMRT. This difference is shown in Fig. 1. After examination of the models it was concluded that the temperature dependencies of both differ significantly. This is shown in Fig. 2 where the temperature dependencies of the two models are shown under high-pressure conditions.

1.2. Water vapor

A successful measurement campaign of water vapor's centimeter-wavelength microwave absorption under a jovian atmosphere was con ducted by Karpowicz and Steffes (2011a,b).

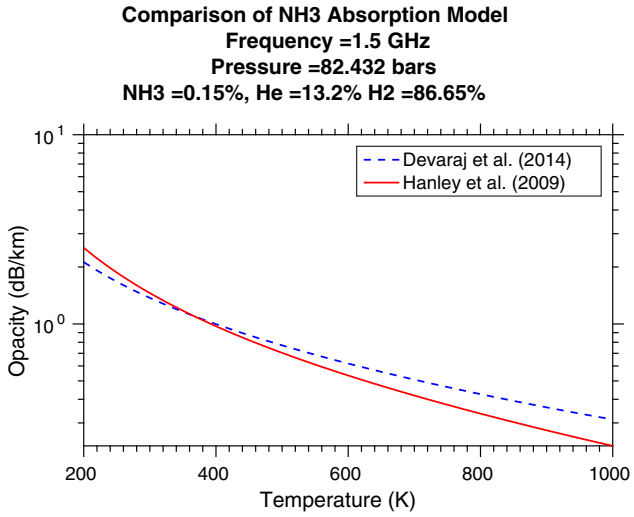

Fig. 2. The temperature dependences of the Devaraj et al. (2014) model and the Hanley et al. (2009) model. Here the pressure, concentration, and frequencies are kept constant.

While nearly 2000 laboratory measurements were conducted at pressures from 30mbars to 101 bars and temperatures up to 525 K, the model developed by Karpowicz and Steffes (2011a,b) produces non-physical results at temperatures greater than 550 K. (That is, the opacity model shows no temperature dependence for temperatures greater than 550 K).

1.3. Methane

A total of 264 microwave opacity measurements of either 100 or 200 mbar ammonia pressure-broadened by up to 3 bars of methane at temperatures ranging from 330 K to 450 K in the 5–20 cm wavelength region have been conducted. A model for this methane-broadening effect has been developed by adjusting the methane-broadening line shape coefficients to obtain a model that best fits the laboratory measurements. This new model complements the newly-developed ammonia model described in this work. In order to verify that the measured effects were only due to the broadening of ammonia's spectrum by methane and not its intrinsic absorption, an additional experiment was conducted using 40 bars of methane mixed with hydrogen to a total pressure of 80 bars. This additional experiment confirmed the microwave transparency of methane.

From experimental data, it has been found that methane will indeed broaden ammonia inversion lines, increasing the microwave opacity of ammonia in the longer centimeter-wavelength region. Through comparisons with previous ammonia line-broadening models, it is found that the broadening parameter for methane is considerably larger than that of hydrogen and helium. Yet, the impact on ammonia opacity of helium and hydrogen is expected to be more significant than that of methane because these constituents are more abundant at Jupiter. Due to methane's relatively low abundance at Jupiter (~0.2% by volume), its effect on the microwave spectrum which will be observed by the Juno MWR will be minimal. However, these experimental results will significantly improve the understanding of the microwave emission spectrum of Uranus and Neptune, where methane is of greater abundance (~2–4% by volume).

2. Measurement theory and system

Verifying the centimeter-wavelength absorption spectrum of microwave absorbing constituents is important for accurate retrievals of constituent abundances in the jovian atmosphere. Conducting measurements under simulated jovian conditions assures the accuracy and usefulness of any model derived from such measurements.

In this experimental program, measurements of the quality factor (Q) of a resonant mode of a resonator are used to determine the absorption of a gas or gas mixture at that resonant frequency (Hanley and Steffes, 2007). The relationship between quality factor and absorption is given by

$$\alpha = 8.686\frac{\pi}{\lambda}\left(\frac{1-\sqrt{t_{loaded}}}{Q^m_{loaded}} - \frac{1-\sqrt{t_{matched}}}{Q^m_{matched}}\right)\text{dB/km} \quad (1)$$

where α is the abso rptivity of the gas (dB/km), λ is the wavelength of the resonance (in km), t is the transmissivity of the resonance, and Q is the quality factor of the resonance. The subscripts *loaded* and *matched* refer to the measurements made with the test gas and pure argon respectively. The full derivation of this equation can be found in Appendix A.

Described below is the laboratory equipment and measurement procedure used in the measurements of gaseous NH_3, H_2O, and CH_4 under simulated deep jovian atmospheric conditions.

2.1. High-temperature and high-pressure centimeter-wavelength measurement system

A high-pressure measurement system was used to conduct measurements of the 5–20 cm-wavelength absorptivity of ammonia and water vapor under deep jovian conditions at temperatures up to 600 K. The high-pressure measurement system consists of a planetary atmospheric simulator, centimeter-wavelength subsystem, and a data handling system.

2.1.1. The planetary atmospheric simulator

The planetary atmospheric simulator was based on one used by Karpowicz and Steffes (2011a,b). The simulator consists of a high-pressure vessel, temperature chamber, temperature and pressure gauges, vacuum pump, various gas bottles, as well as gas handling valves and pipes. The main component of the planetary atmospheric simulator is a high-pressure vessel that operates at pressures up to 100 bars and temperatures up to 525 K. The pressure vessel's maximum pressure can be de-rated to 80 bars at 600 K. This is placed in a Grieve industrial oven (model AB-650 rated up to 615 K). The oven acts as a stable temperature chamber and maintains the temperature within ±0.5 °C. The oven is placed on an outdoor concrete pad and enclosed by a metallic shed for protection.

Ultra-high-purity UHP300 grade Airgas bottles (pre-mixed hydrogen/helium, ammonia, methane and argon) required for the measurements are placed on a gas cylinder rack adjacent to the shed. Pressure regulators control the gas delivery to the system through Manifold Swagelok fittings and seamless stainless steel tubing. An exhaust valve is used to vent the gases to ambient pressure, and a Welch DuoSeal vacuum pump model 1376B-01 is used to evacuate the pressure vessel from ambient pressure down to vacuum (better than 0.1 mbar).

A GE Druck DPI 10430A Digital Test Gauge is used for pressure sensing in the 0 to 2 bar range, and a GE Druck DPI 1043000A Digital Test Gauge is used for pressure sensing in the 2–200 bar range. An Omega resistance temperature detector RTD (PR-11-2-100-1/4-9-E) is used for sensing gas temperature in the pressure vessel. A block diagram of the various components of the simulator is shown in Fig. 3.

2.1.2. Centimeter-wavelength subsystem

A type 304 stainless steel cylindrical cavity resonator with gold-plated interior is placed inside the ultra-high pressure

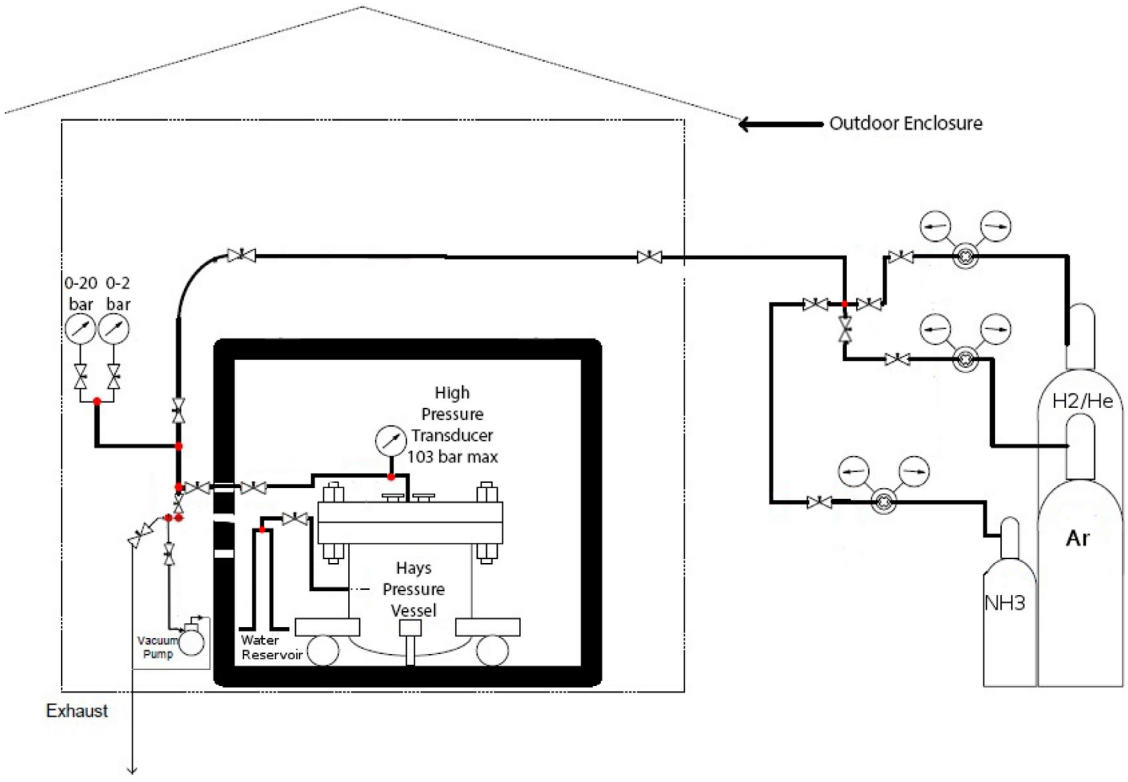

Fig. 3. The Georgia Tech high-pressure system used for studying the centimeter-wavelength properties of ammonia under simulated jovian conditions.

vessel. The interior of the cavity resonator measures approximately 13.1 cm in diameter and 25.5 cm in height. One dozen high-Q, low-asymmetry resonances in the 5–20 cm wavelength range were selected and used as "standard resonances" for all the measurements. A detailed description of the selection criteria for the resonances is provided by Hanley et al. (2009).

Ceramtec microwave feedthroughs model 16545-01-CF are used for coupling microwave energy through the top-plate of the pressure vessel to the resonator via Times Microwave high-temperature (SiO_2) cables. The cables are rated up to 875 K and the feedthroughs are rated to 103 bars and 625 K. Exterior to the pressure vessel, two 1 m long sections of the same cable are connected to two sections of 25 m length Andrews CNT 600 microwave cable outside the oven. These are connected to an Agilent E5071C vector network analyzer that is placed inside the laboratory environment to ensure temperature stability. The network analyzer S-parameter measurements are recorded by the data acquisition system via General Purpose Interface Bus (GPIB).

2.1.3. Data acquisition subsystem

The data acquisition subsystem consists of a laptop computer connected to the network analyzer and a digital multimeter via GPIB. The extended USB buses allow the computer to remain inside the laboratory. The network analyzer is controlled via MATLAB® software. The software used is similar to that used by Hanley and Steffes (2007) and a detailed description of the data acquisition system is provided by Karpowicz and Steffes (2011a). A block diagram of the various components of the simulator is shown in Fig. 4.

2.2. Measurement procedure

The most important prerequisite for performing measurement of gas properties is ensuring a leak-proof system. Pressure integrity was verified using two methods: the first is by drawing a vacuum inside the pressure vessel and verifying the integrity of the vacuum over time. The second is by adding a positive pressure of Argon to the system and ensuring there are no leaks in any of the connectors and valves. Ensuring a leak-proof system allows for not only precise measurements but also that no toxic gases are released into the testing environment.

After the system is established to be leak-proof and at a stable temperature, a vacuum is drawn and measurement is taken. This allows for a baseline measurement of the cavity resonator's resonances and their quality factors. Once this baseline is established, the gas under test is added to the system.

Once the gas temperature has stabilized, another set of tests measuring the resonant frequencies along with the quality factors is taken. More gas is added and the procedure is repeated until measurements at all suitable pressures are taken. A vacuum is then drawn for an extended period (12 h) to minimize the possibility of adsorption (or "sticking") of the gas being tested (NH_3) to metal surfaces inside the vessel. This second vacuum measurement is taken to measure any possible system drift.

Once the second vacuum measurement is taken, a microwave transparent gas (Argon) is then added to the vessel until the center frequencies of the resonances are matched to the same frequency as with the test gas. Again measurements are taken and this is repeated for every pressure of the test gas. Once completed, a vacuum is again drawn and another test is taken.

Lastly, it is important to account for the loss in the long microwave cables and the connectors between the network analyzer and the resonator. Three sets of straight-through measurements of signal levels are made (without the resonator present) under the same temperature conditions at each frequency point of the test gases. This loss is used to correct the measurements of the transmissivities (Eq. (A.5)) of the test gases and the dielectric matching gas.

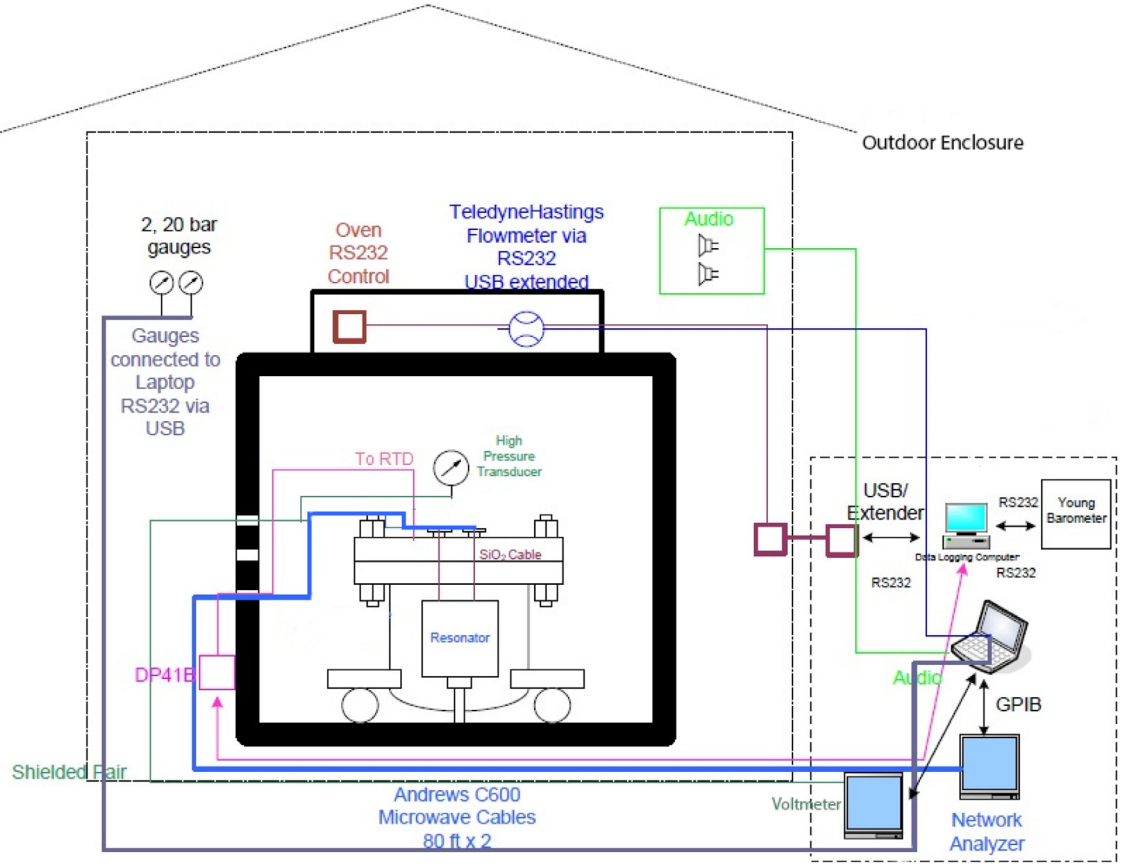

Fig. 4. The centimeter-wavelength subsystem and the data-acquisition components of the high-pressure system.

The measurements include disconnecting the Andrews CNT 600 microwave cables from the Times Microwave high-temperature cables and connecting them via a SMA jumper cable. The loss of the SMA jumper cable, Times Microwave high-temperature cable, and Ceramtec microwave feedthroughs are well characterized and used to adjust the signal level measured. The connections are disconnected and reconnected between each set of transmissivity measurement in order to better statistically characterize the reproducibility of the electrical connections (Devaraj et al., 2011).

2.2.1. Data processing

Data processing is performed after each measurement cycle using software written in MATLAB®. The software used is similar to that described in Hanley and Steffes (2007) and Karpowicz and Steffes (2011a), but with some modifications to account for the new configuration of the system. The software reads, processes, and calculates the absorptivity of the test gas. The cable losses at each measurement point are calculated by taking the mean of 30 sweeps of the signal level then averaging the three sets of the measurement. The test gas insertion loss and dielectrically matched insertion loss are obtained by subtracting the cable loss from the peak power measurements of both the test gas and the dielectrically matched gas.

The uncertainties associated with the measurements are: (i) instrumental errors (Err_n), (ii) errors in dielectric matching (Err_{diel}), (iii) transmissivity or signal-level errors (Err_{trans}), (iv) errors due to asymmetry in resonances (Err_{asym}), and (v) errors in measurement conditions (Err_{cond}) due to uncertainties in the pressure, temperature, and concentration measured (Hanley and Steffes, 2007; Karpowicz and Steffes, 2011a,b). Since Err_{cond} does not directly affect the microwave absorptivity measurements, this uncertainty is kept separate from Err_{tot}. The 95% confidence Err_{tot} is calculated as per Hanley et al. (2009)

$$Err_{tot} = \sqrt{Err_n^2 + Err_{diel}^2 + Err_{trans}^2 + Err_{asym}^2} \quad (2)$$

Although uncertainties in measurement conditions do not directly affect the measurements of absorptivity, they still need to be accounted for when evaluating the opacity formalisms. It is computed by

$$Err_{cond} = \sqrt{Err_{temp}^2 + Err_p^2 + Err_c^2} \quad (3)$$

with Err_{temp}, Err_p, and Err_c representing the 2σ uncertainties of the measured opacity resulting from variations in temperature, pressure, and concentration (or mole fraction), respectively. Each of these are calculated by taking the maximum modeled opacity with each uncertainty minus the minimum modeled opacity and halving the difference.

3. Measurement results

High accuracy laboratory measurements of the centimeter-wavelength absorption of gaseous ammonia and water vapor at high temperatures, and for gaseous ammonia when pressure broadened by methane, have been conducted. These three measurement campaigns consist of over 300 laboratory measurements using the system described previously. This section discusses the details of each campaign.

3.1. Ammonia

Previous measurement campaigns have involved laboratory measurements of the opacity of ammonia under simulated deep

jovian conditions at pressures up to 100 bars and temperatures up to 500 K (Devaraj et al., 2014). This work has extended the temperature range to nearly 600 K. Since the pressure seals of the system had limited performance at such high temperatures, only measurements of the absorptivity of pure ammonia (0.5 bar pressure) were completed. The UHP (Ultra-High Purity) grade ammonia used in the measurements of absorptivity and the UHP grade argon used for the dielectric matching process were provided by Airgas, Inc.

The measurement of ammonia's absorption began by adding 500 mbar of ammonia to an evacuated pressure chamber heated to 595 K. The gas was allowed to heat up and measurements of its absorptivity and refractivity were made. The chamber was then evacuated and the dielectric matching process with argon gas was conducted.

3.2. Water vapor

Similar to ammonia, previous measurement campaigns have measured the 5–20 cm opacity of water vapor under simulated deep jovian conditions. These measurements reached pressures up to 100 bars and temperatures up to 525 K (Karpowicz and Steffes, 2011a,b). This work has extended the temperature range. Measurements of pure water vapor have been made in the 3.5–4.7 bar range.

To measure the opacity of water vapor, reverse osmosis, deionized (RO/DI) liquid water was inserted into the evacuated, heated chamber through a high-pressure clear rubber hose. To reach pressures above ambient, UHP grade argon was used to pump the liquid water through the hose and into the chamber. The clear hose served as a window to ensure that no argon was added to the chamber. To ensure that no water vapor condensed when the pressure was measured with the pressure sensor at ambient temperature, the pipes in the gas manifold were filled with 10 bars of argon to prevent water vapor from exiting the heated chamber. Since the volume of the pipes was quite small, this had a negligible effect on the accuracy of the pressure measurement. After the opacity and refractivity were measured, some water vapor was immediately released and another measurement was taken. The chamber was evacuated over a period of 15 h to minimize adsorption, but it was noticed that the quality factor of all the resonances at a vacuum were drastically lower than previous vacuum measurements. This was caused by damage to the resonator probes as the system was evacuated under these extremely high temperature conditions. Due to the decrease in the vacuum quality factor, reliable dielectric matching could not be conducted. As a result, a differential measurement was conducted by comparing the quality factors with 4.734 bars of water vapor present versus that with 3.612 bar pressure.

Using Eq. (A.3) the differential opacity is calculated by

$$\alpha_{p_1} - \alpha_{p_2} = \frac{\pi}{\lambda}\left(\frac{1}{Q_{gas,p_1}} - \frac{1}{Q_{gas,p_2}}\right) \tag{4}$$

where p_1 and p_2 represent the two different pressures, α is the opacity (in dB/km) and Q_{gas} quality factor of the resonance. Substituting Eq. (A.8) into Eq. (4) gives

$$\alpha_{p_1} - \alpha_{p_2} = \frac{\pi}{\lambda}\left(\frac{1-\sqrt{t_{loaded,p_1}}}{Q_{loaded,p_1}} - \frac{1-\sqrt{t_{loaded,p_2}}}{Q_{loaded,p_2}}\right) \tag{5}$$

where p_1 and p_2 are the two different pressures, t_{loaded} is the measured transmissivity as per Eq. (A.5) and Q_{loaded} is the measured quality factor of a resonance in the presence of water vapor at the stated pressure.

While differential measurements have larger uncertainties, due to lack of dielectric matching, these measurements were useful to verify the validity of the revised model for water vapor opacity.

3.3. Methane

An additional measurement campaign has been conducted to develop a model for the opacity of ammonia when pressure-broadened by methane in the 5–20 cm wavelength region. A total of 264 laboratory measurements in the 330–450 K temperature range were performed from February through to April of 2012, and the necessary line shape coefficients have been determined to best fit the opacity data. The UHP (Ultra-High Purity) grade ammonia and methane used to take measurements of absorptivity and the UHP grade argon used for the dielectric matching process were all provided by Airgas, Inc.

The measurement of ammonia's absorptivity when broadened by methane begins by first adding ammonia at either 100 or 200 mbar pressure to an evacuated pressure vessel containing a cylindrical cavity resonator at the desired temperature within the range of 330–450 K. The absorption spectrum of the gas in the pressure vessel is then pressure-broadened by adding methane giving a total pressure of 1, 2 and 3 bars. Measurements of absorptivity and refractivity are made with pure ammonia and again with each addition of methane gas. The chamber is evacuated before the dielectric matching process with argon gas is conducted. The measurements of the pressure-broadened ammonia serve as a basis for the development of the model which will accurately determine the role of methane in the microwave absorption of ammonia. Each of the 264 measurements taken represents a different combination of frequency, mixing ratio, temperature and pressure. Table 1 illustrates the sets of measurements taken in this work.

Another set of laboratory measurements was collected with the objective of determining limits to the microwave opacity of methane in the 5–20 cm wavelength region at the temperature of 295 K. For this experiment, methane is the test gas. It was further pressure-broadened by hydrogen in the high-pressure system. This set of laboratory experiments was performed from May through to June of 2012. Similar to the ammonia broadening experiment, the gas bottles were provided by Airgas, Inc. The methane and hydrogen used in the absorptivity measurements were of UHP (Ultra-High Purity) grade as was the argon used for the dielectric matching process.

Methane's microwave absorptivity was measured by first adding 40 bars of methane to the evacuated pressure chamber containing the cylindrical cavity resonator. At the desired temperature of

Table 1
Summary of the ammonia/methane experiments conducted at centimeter-waves.

Experimental dates	Temperature range (K)	Nominal pressure (bar) and {NH_3 concentration (%)}
02/2012	449.3–449.7	0.097 {100}, 0.996 {9.77}, 2.002 {4.86}, 3.008 {3.23}
02/2012 – 03/2012	449.6–449.8	0.203 {100}, 0.999 {20.28}, 2.006 {10.10}, 3.010 {6.73}
03/2012	374.6–374.7	0.100 {100}, 1.000 {10.03}, 2.006 {5.00}, 3.001 {3.34}
03/2012	374.6–374.7	0.198 {100}, 1.000 {19.83}, 2.001 {9.90}, 3.017 {6.57}
03/2012 – 04/2012	329.3–329.7	0.107 {100}, 0.999 {10.67}, 2.000 {5.33}, 3.006 {3.55}
04/2012	329.6–329.8	0.201 {100}, 1.001 {20.08}, 1.998 {10.06}, 3.012 {6.67}

Table 2
Measured upper limit of the centimeter-wavelength absorption of 40 bars of pure methane.

Center frequency (GHz)	Wavelength (cm)	Upper limit (dB/km)
1.4849	20.189	0.033597
1.7852	16.793	0.126596
2.1962	13.651	0.08965
2.7576	10.871	0.228918
3.0399	9.8619	0.464194
3.3959	8.8281	0.881919
4.0229	7.4521	0.255788
4.2518	7.051	0.409156
5.0021	5.9933	1.171127
5.2194	5.7438	0.332237
5.8468	5.1275	0.645721
5.9855	5.0086	2.63271

Table 3
Measured upper limit of the centimeter-wavelength absorption of 80 bars of a methane–hydrogen mixture.

Center frequency (GHz)	Wavelength (cm)	Upper limit (dB/km)
1.4776	20.3	0.070936
1.7764	16.89	0.175947
2.1854	13.73	0.051405
2.744	10.93	0.396851
3.0249	9.918	0.836497
3.3792	8.878	1.025798
4.0031	7.494	0.14976
4.2309	7.091	0.40037
4.9775	6.027	0.846399
5.1937	5.776	0.810677
5.9561	5.0369	7.740521

295 K, the opacity measurements were collected. This gas was then pressure-broadened by 40 bars of hydrogen, bringing the total pressure to 80 bars within the resonator, and a second set of measurements was taken. A vacuum was then drawn in the pressure vessel containing the resonator. Argon was then added to match the refractive index of the pure methane at 40 bars. Since it is also a microwave transparent gas, additional hydrogen gas was added to dielectrically match the measurements of the methane–hydrogen mixture taken at 80 bars. A total of 23 measurements were collected; 12 of pure methane at the pressure of 40 bars and another 11 of the methane–hydrogen mixture at the pressure of 80 bars. As shown in Tables 2 and 3, the measurements taken in this experiment confirmed the microwave transparency of methane. A comparison of the upper-limit of the opacity of the 80 bar methane–hydrogen mixture and the modeled opacity of 1 bar of pure ammonia is shown in Fig. 5.

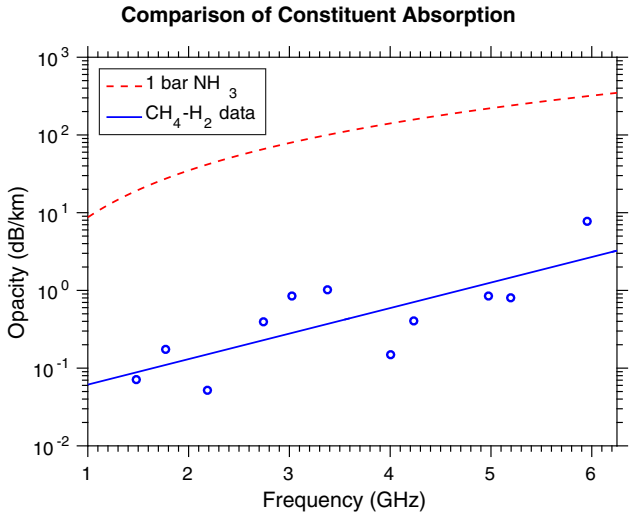

Fig. 5. Measured upper limits of the centimeter-wavelength absorption of 80 bars of a methane–hydrogen mixture compared to the modeled absorption of 1 bar of pure Ammonia at a temperature of 295 K. The solid line is a log average of the upper-limit of the measured opacity of the methane–hydrogen mixture. No statistically significant absorption was measured.

4. Revisions to existing models

New models for the absorption of gaseous ammonia and water vapor at high temperatures and gaseous ammonia when pressure broadened by methane have been developed. This section describes the data fitting process and the resulting models for each constituent.

4.1. Ammonia

The primary goal of this work has been to develop an ammonia model that adheres to strict physical principals. While previous models (Devaraj et al., 2014; Hanley et al., 2009) of ammonia's centimeter- and millimeter-wave absorption fit the available laboratory measurements, anomalous behavior of these models when extrapolated to higher temperatures shows that their examination from a physical viewpoint is needed.

The model created by Hanley et al. (2009) has three distinct weaknesses: (i) No high pressure and/or high temperature data was used in the model development, (ii) Only one H_2/He mixing ratio was used, and (iii) the model employed an outdated line catalog. When the Hanley model was developed, only data with pressures at or less than 12 bars and temperatures at or less than 450 K were used to fit the model. While the H_2/He mixing ratio (86.3%/13.7%) used was characteristic of Jupiter, it does not apply to all outer planets. By not varying the H_2/He mixing ratio the model was required to assume Helium parameters from Berge and Gulkis (1976), which were not directly measured. The line catalog used by Hanley et al. (2009) only has 190 lines while the current one has 5914 lines (Yu et al., 2010a,b,c).

Similarly the Devaraj et al. (2014) model has a number of physical weaknesses: (i) the temperature dependence of the coupling parameters (Z_i) were unnecessarily limited during model creation, (ii) the rotational line parameters are unnecessarily coupled to the inversion line parameters, (iii) in the high pressure model, the shift parameter (δ_j) of the inversion lines is positive, and (iv) a significant discontinuity occurs in the model at the pressure where the parameters are "switched". Limiting the temperature dependence of the coupling parameter (i) directly limits the search space of the fitting function for the model parameters. The positive shift parameter (iii) is nonphysical because inversion lines must be shifted lower in frequency with increasing pressure (Townes and Schawlow, 1975).

When fitting the coefficients for the new model, special steps have been taken to address these issues. The new model uses all the data available (Hanley et al., 2009; Devaraj et al., 2014, and the high temperature data presented in this work). This addresses the limited pressure, temperature, and mixing ratio issues present in the development of the Hanley et al. (2009) model. When fitting the model, the temperature dependence of the coupling parameters are now unbounded (Rosenkranz, personal communicating, August 2015) and the rotational line parameters are not coupled to those from the inversion lines when fitting the new model. The pressure switch present in the Devaraj et al. (2014) model (iv) has been converted to a frequency switch with a much smaller discontinuity.

The data fitting process employed is similar to the one used by Hanley et al. (2009). Ammonia opacity measurements in the 75–150 GHz at pressures up to 3 bars and temperatures up to 300 K made by Devaraj et al. (2011), the high-pressure measurements in the 1.5–6 GHz at pressure up to 100 bars and temperatures up to 500 K made by Devaraj et al. (2014), the 1.5–27 GHz measurements a pressures up to 12 bars and temperatures from 184 K to 450 K made by Hanley et al. (2009), and the high-temperature measurements in the 1.5–6 GHz range made as part of this work were utilized for the data fitting process. Similarly to Hanley et al. (2009) and Devaraj et al. (2014) a data set consisting of 250 data points in the 22–40 GHz range using a Fabry–Perot resonator (FPR) at room temperature and pressures up to 3 bars was used as an independent test set to verify the validity of the model. The Limited-memory BFGS (Broyden–Fletcher–Goldfarb–Shanno) with simple box constraints (L-BFGS-B) optimization technique (Byrd et al., 1995) is used in this work, and has a minimization function

$$\chi = \frac{DW \times (\alpha_{measured} - \alpha_{model})^2}{Err^2_{measured}} \tag{6}$$

where DW is the data weight assigned to the data point, $\alpha_{measured}$ is the measured opacity, α_{model} is the modeled opacity, and $Err_{measured}$ is the measured 2σ uncertainty in opacity calculated as

$$Err_{measured} = Err_{tot} + Err_{cond} \tag{7}$$

where Err_{tot} is the total 2σ measurement uncertainty and Err_{cond} is the 2σ uncertainty due to measurement conditions. Multiple iterations of the minimization function with random initial inputs were run to ensure a global minimum was reached. The data weight is given as (Hanley et al., 2009)

$$DW = \frac{1}{n_f} + \frac{1}{n_T} + \frac{1}{n_P} + \frac{1}{n_C} \tag{8}$$

where n_f, n_T, n_P, and n_C represent the number of measurements conducted at each frequency, temperature, pressure, and gas concentration range. The data points are divided into roughly equally spaced fTPC bins and scaled to prevent the model from being skewed toward the most frequently measured conditions.

The data was then split into two groups. Group I is data where frequency is less than 24 GHz and Group II is data where frequency is greater than 24 GHz. The inversion lines are fit to a Ben-Reuven lineshape using only data from Group I. 2618 data points are used to fit the 14 free inversion parameters. The data in Group II was best fit with the low pressure model already presented in Devaraj et al. (2014).

4.1.1. New ammonia absorption formalism

Laboratory measurements were used to develop a consistent mathematical formalism that can be used to estimate the opacity of ammonia under jovian conditions. The following is described in depth by Devaraj et al. (2011), but will be briefly discussed here for completeness. The absorption of a gas is modeled by

$$\alpha = \sum_j A_j \pi \Delta\nu_j F_j(\nu, \nu_{(0,j),\ldots}) \tag{9}$$

where j represents the line index, A_j represents the absorption at the line center in cm^{-1}, $\Delta\nu_j$ represents the linewidth in cm^{-1}, $F_j(\nu, \nu_{0,j})$ represents the lineshape function in cm, ν represents the frequency of the incident electromagnetic wave in cm^{-1}, and $\nu_{(0,j)}$ represents the frequency at the line center in cm^{-1} (Townes and Schawlow, 1975). The absorption at each line center is calculated using information from the latest JPL catalog, version 5, updated on September 2010 (Yu et al., 2010a,b,c) as per Pickett et al. (1998). The absorption at the line center is represented by

$$A_j = \frac{nI_j(T)}{\pi \Delta\nu_j} \ (cm^{-1}) \tag{10}$$

where n is the number density of the gas in molecules/cm^3 and $I_j(T)$ is the intensity of the line in cm^{-1}/(molecules/cm^2) at temperature T in Kelvins.

The NH_3 inversion, rotational, and roto-vibrational lines were obtained from the JPL Spectral line catalog (Pickett et al., 1998). A modified Ben-Reuven lineshape (Ben-Reuven, 1966) was used for the inversion transitions and a modified Gross lineshape (Gross, 1955) was used for the rotational and robo-vibrational transitions. Line transitions where no broadening parameters were available were made free parameters and were derived for this work.

The cumulative ammonia opacity from the inversion, rotational, and roto-vibrational transitions is calculated by

$$\alpha = (\alpha_{inv} + \alpha_{rot} + \alpha_{\nu_2}) \times 434294.5 \ (dB/km) \tag{11}$$

where α_{inv}, α_{rot}, and α_{ν_2} are the opacities from the inversion, rotational, and roto-vibrational lines in cm^{-1}. The factor 434294.5 converts the total opacity from cm^{-1} to dB/km.

A detailed description of the opacity calculations for the rotational and roto-vibrational lines is given by Devaraj et al. (2011). Since the roto-vibrational, and rotational transitions of ammonia occur in the millimeter-wavelength range, and the jovian atmospheric layers that contribute to emissions at these frequencies have pressures less than a few bars (Joiner and Steffes, 1991), using this model (low pressure Devaraj et al., 2014) as a high frequency model follows physical principals. A new set of inversion model parameters have been found to better fit the data at centimeter-wavelengths. The opacity from the ensemble of inversion lines is given by

$$\begin{aligned}\alpha_{inv} = {} & \frac{0.1 D_{inv} P_{NH_3}}{k_b T}\left(\frac{2}{\pi}\right)\left(\frac{T_0}{T}\right)^{\eta+1} \\ & \times \sum_j \left(I_j(T_0) \exp\left(\left(\frac{1}{T_0} - \frac{1}{T}\right) E_{(I,j)}\left(\frac{hc}{k_B}\right)\right)\left(\frac{\nu}{\nu_{(0,j)}}\right)^2 \right. \\ & \left. \times \left[\frac{(\gamma_j - \zeta_j)\nu^2 + (\gamma_j + \zeta_j)\left[(\nu_{(0,j)} + \delta_j)^2 + \gamma_j^2 - \zeta_j^2\right]}{\left[\nu^2 - (\nu_{(0,j)} + \delta_j)^2 - \gamma_j^2 + \zeta_j^2\right]^2 + 4\nu^2\gamma_j^2} \right] \right)\end{aligned} \tag{12}$$

Where for inversion line j, $\nu_{(0,j)}$, γ_j, ζ_j, and δ_j are the center frequency, linewidth, coupling parameter, and shift parameter, respectively, in cm^{-1}, and D_{inv} is a unitless scale factor. The frequency, linewidth, coupling, and shift parameters are converted from GHz to cm^{-1} before they are used. The linewidth and coupling parameters are calculated by summing the contributions from ammonia, hydrogen, and helium. The linewidth and coupling parameters are given by

$$\begin{aligned}\gamma_j = {} & \gamma_{H_2} P_{H_2}\left(\frac{300}{T}\right)^{\Gamma_{H_2}} + \gamma_{He} P_{He}\left(\frac{300}{T}\right)^{\Gamma_{He}} \\ & + \gamma_{NH_3}\gamma_{(0,j)} P_{NH_3}\left(\frac{295}{T}\right)^{\Gamma_{NH_3}} \ (GHz)\end{aligned} \tag{13}$$

$$\begin{aligned}\zeta_j = {} & \zeta_{H_2} P_{H_2}\left(\frac{300}{T}\right)^{Z_{H_2}} + \zeta_{He} P_{He}\left(\frac{300}{T}\right)^{Z_{He}} \\ & + \zeta_{NH_3}\gamma_{(0,j)} P_{NH_3}\left(\frac{295}{T}\right)^{Z_{NH_3}} \ (GHz)\end{aligned} \tag{14}$$

where for inversion line j and constituent $i = H_2$, He, NH_3, γ_i and ζ_i are constant scale terms (in GHz/bar), and Γ_i and Z_i represents the constant temperature dependences of the broadening of each

Table 4
Values of the low-frequency inversion model constants used for computing the H_2/He-broadened NH_3 absorptivity when $f \leq 30$ GHz.

	i=H_2	i=He	i=NH_3	Units
γ_i	1.6937	0.6997	0.7523	(GHz/bar)
Γ_i	0.8085	1.0	1.0	
ζ_i	1.3263	0.1607	0.6162	(GHz/bar)
Z_i	0.8199	−0.7269	1.3832	
d		−0.0139		
D_{inv}		0.9619		

Table 5
Values of the high-frequency inversion model constants used for computing the H_2/He-broadened NH_3 absorptivity when $f > 30$ GHz.

	i=H_2	i=He	i=NH_3	Units
γ_i	1.7465	0.9979	0.7298	(GHz/bar)
Γ_i	0.8202	1.0	1.0	
ζ_i	1.2163	0.0291	0.5152	(GHz/bar)
Z_i	0.8873	0.8994	2/3	
d		−0.0627		
D_{inv}		0.9862		

Table 6
Values of the model constants of the new model used for computing the H_2/He-broadened NH_3 absorptivity from the rotational transitions (Devaraj et al., 2011).

	i=H_2	i=He	i=NH_3
c_i	1.7761	0.6175	3.1518
ξ_i	0.5	0.5663	1.0
D_{rot}		2.7252	

of the gases, P_i are the ideal partial pressures in bar, and $\gamma_{(0,j)}$ are the self-broadening linewidths of the inversion transitions of ammonia in MHz/Torr and the conversion to GHz/bar is incorporated in the scale terms γ_{NH_3} and ζ_{NH3}. The values for $\gamma_{(0,j)}$ are from the calculations of Poynter and Kakar (1975) assuming a T_0 of 295 K. For the lines with a center frequency below 7.2 GHz and $J > 16$, where J represents the total angular momentum vector for the ammonia molecule, γ_0 is expressed as

$$\gamma_0(J,K) = 25.923\frac{K}{\sqrt{J(J+1)}}\ (\text{MHz/Torr}) \tag{15}$$

where K is the projection of J onto the molecular axis. The pressure shift parameter is calculated by

$$\delta_j = d \times \gamma_i \tag{16}$$

where d is an empirically derived constant. All the inversion lines are assigned the same set of model constants (either low-frequency or high-frequency) even though each line behaves differently (Hanley et al., 2009). The equation for computing the opacity from the inversion transitions has 14 free parameters. A new set of free-parameters for the centimeter-wavelength inversion transitions have been empirically derived by data fitting as shown in Table 4. Table 5 shows the millimeter-wavelength effects of the inversion transitions to be identical to the values calculated by Devaraj et al. (2011). The rotational and roto-vibrational transitions from Devaraj et al. (2011) are shown in Tables 6 and 7 respectively.

Due to the asymmetry of the Ben-Reuven lineshape it was decided that the frequency switch should be in the range between 25–70 GHz. Using the weighting functions for the jovian planets at frequencies from 25–70 GHz, the appropriate search space for

Table 7
Values of the model constants of the new model used for computing the H_2/He-broadened NH_3 absorptivity from the roto-vibrational transitions (Devaraj et al., 2011).

	i=H_2	i=He	i=NH_3	Units
$\Delta\nu_i$	0.5982	0.6175	5.0894	(GHz/bar)
ξ_i	0.5	0.5505	0.9996	
D_{ν_2}		0.7286		

Table 8
Values of the parameter search space used in the Monte-Carlo switch minimization algorithm.

Pressure:	0–7 bars
Temperature:	100–250 K
Ammonia concentration:	0–0.2%
Helium concentration:	10–20%

pressure, temperature, ammonia concentration, and helium concentration have been identified and are shown in Table 8. A Monte-Carlo method was used to explore this search space to minimize the difference between the two inversion models. Multiple simulations indicate that a frequency switch located at 30 GHz had the smallest average model discontinuity.

4.1.2. Model performance

Model performance is evaluated based on the fit to the data over the parameter space where the model is effective. (Note: The model uses the low-frequency inversion line parameters at $f \leq 30$ GHz and a high-frequency inversion line parameters at $f > 30$ GHz). The model was compared with the 11 data points of the 1.5–6 GHz high temperature data measured in this work, the 1431 data points of the 1.5–27 GHz opacity of ammonia and the 250 data points of the 22–40 GHz opacity of ammonia measured by Hanley et al. (2009), 1013 data points of the 75–150 GHz opacity of ammonia measured by Devaraj et al. (2011), and the 1176 data points of the 1.5–6 GHz opacity of ammonia measured by Devaraj et al. (2014).

This new ammonia opacity model fits 100% of the high-temperature cavity resonator measurements, 95.94% of the 1.5–27 GHz cavity resonator measurements, 89.2% of the 22–40 GHz FPR measurements, 80.36% of the 75–150 GHz FPR measurements, and 70.23% of the 1.5–6 GHz high-pressure measurements. Comparison of the new model performance with models of Hanley et al. (2009) and Devaraj et al. (2014) is listed in Table 9. Fig. 6 shows the high temperature data compared to various models.

Similar to the model developed by Devaraj et al. (2014), the model presented in this work diverges from the Hanley et al. (2009) model when extrapolated to extreme temperatures. This model is quite similar to the one developed by Devaraj et al. (2014) when extrapolated to high temperatures and high pressures of broadening gases. The major differences between this model and the Devaraj et al. (2014) model occur at 15 bars (the "switching" pressure of the Devaraj et al. (2014) model) and at high temperatures when there are no broadening gases present (as shown in Fig. 6).

4.2. Water vapor's influence on ammonia's absorption spectrum

Devaraj et al. (2014) conducted the first laboratory measurement campaign to measure water vapor's broadening of the 5–20 cm-wavelength opacity of ammonia over a range of jovian conditions. While, the model described previously in this section only accounts for broadening due to hydrogen and helium, a simple modification to this model can account for water vapor's broadening of ammonia's absorption spectrum.

Table 9
The percentage of the ammonia opacity measurement data points within 2σ uncertainty of the new model in comparison with the existing models.

Model	Cavity (1.–27 GHz)	FPR (22–40 GHz)	FPR (75–150 GHz)	High pressure (1.5–6 GHz)	High temperature (1.5–6 GHz)	Total
Hanley et al. (2009)	95.88	86.0	13.03	65.14	100.00	64.31
Devaraj et al. (2014)	93.92	90.8	80.36	70.92	45.46	83.07
This work	**95.94**	**89.2**	**80.36**	**70.32**	**100.00**	**83.68**

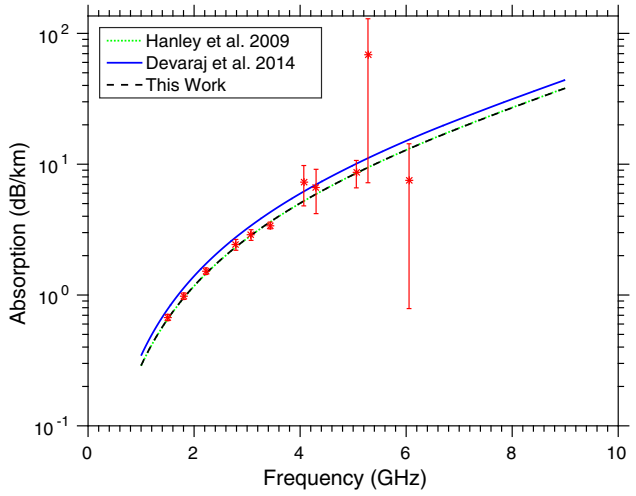

Fig. 6. Opacity data measured using the high-temperature centimeter-wavelength system for pure NH_3 at a pressure of 0.5 bar and temperature of 595 K compared to various models. It is important to note that This work and the Hanley et al. (2009) models are overlapping.

Pure ammonia's opacity due to inversion transitions is modeled with a modified Ben-Reuven line shape described previously in this work. The relationship for the opacity due to inversion lines is shown in Eq. (12). The linewidth and coupling parameters are modified by adding the contribution of water vapor to Eqs. (13) and (14) as follows

$$\gamma_j = \gamma_{H_2O} P_{H_2O}\left(\frac{300}{T}\right)^{\Gamma_{H_2O}} + \gamma_{H_2} P_{H_2}\left(\frac{300}{T}\right)^{\Gamma_{H_2}} + \gamma_{He} P_{He}\left(\frac{300}{T}\right)^{\Gamma_{He}} + , \gamma_{NH_3}\gamma_{(0,j)} P_{NH_3}\left(\frac{295}{T}\right)^{\Gamma_{NH_3}} \text{ (GHz)} \quad (17)$$

$$\zeta_j = \zeta_{H_2O} P_{H_2O}\left(\frac{300}{T}\right)^{Z_{H_2O}} + \zeta_{H_2} P_{H_2}\left(\frac{300}{T}\right)^{Z_{H_2}} + \zeta_{He} P_{He}\left(\frac{300}{T}\right)^{Z_{He}} + \zeta_{NH_3}\gamma_{(0,j)} P_{NH_3}\left(\frac{295}{T}\right)^{Z_{NH_3}} \text{ (GHz)} \quad (18)$$

where for the inversion line j and constituent $i = H_2O$, H_2, He, NH_3, γ_i and ζ_i are constant scale terms, and Γ_i and Z_i represents the constant temperature dependences of the broadening of each of the gases, P_i are the ideal partial pressures in bar, and $\gamma_{(0,j)}$ are the self-broadening linewidths of the inversion transitions of ammonia in MHz/Torr.

Prior to fitting the measured data points to the model for ammonia opacity, the intrinsic opacity of the water vapor–hydrogen–helium mixture must be removed. Using the modified Karpowicz and Steffes (2011a,b) model described in Section 4.3, the intrinsic opacity of water vapor present in each experiment was removed. Subsequently, data fitting and optimization were performed in a fashion similar to that explained previously. The ammonia, hydrogen, and helium free parameters for the linewidth and coupling parameters are described previously in this work. Water vapor's free parameters are displayed in Table 10.

Table 10
Constants of H_2O-broadening of NH_3

	i=H_2O	Units
γ_i	5.3119	(GHz/bar)
Γ_i	0.6224	
ζ_i	5.2333	(GHz/bar)
Z_i	2.1248	

The new model fits 66.3% of the 838 data points within 2σ. This is an improvement of 2.5% from the Devaraj et al. (2014) model.

4.3. Water vapor

A new model for the intrinsic opacity of water vapor has been developed which is a modification of the model created by Karpowicz and Steffes (2011a,b). This model has two distinct parts, the absorption due to individual resonant lines and the absorption due to water vapor's continuum. While the former is important, it is less significant in the frequency range where the Karpowicz and Steffes (2011a); 2011b) laboratory measurements were conducted. At long wavelengths, the absorptivity is dominated by the continuum absorption, defined as

$$\alpha_{continuum} = \alpha_{c,w} + \alpha_{c,f} \quad (19)$$

where $\alpha_{c,w}$ is the continuum term based solely on the water vapor density (self-continuum), and $\alpha_{c,f}$ is the continuum term dependent on the foreign gas influence on the water vapor. As per Rosenkranz (1998), the water vapor self-continuum term is defined as

$$\alpha_{c,w} = C_w P^2_{ideal,H_2O} \Theta^{x_{w,continuum}} f^2 \quad (\text{km}^{-1}) \quad (20)$$

where C_w is an empirically derived constant, $x_{w,continuum}$ is the temperature exponent of the continuum, P_{ideal,H_2O} is the ideal pressure of water vapor (in mbars), $\Theta_{continuum}$ is the standard $\frac{300}{T}$ where T is in degrees Kelvin, and f is the frequency in GHz. Also as per Rosenkranz (1998) and Karpowicz and Steffes (2011a) define the foreign gas contribution as

$$\alpha_{c,f} = C_{H_2} P_{ideal,H_2} P_{ideal,H_2O} \Theta^3 f^2 + C_{He} P_{ideal,He} P_{ideal,H_2O} \Theta^3 f^2 \quad (\text{km}^{-1}) \quad (21)$$

where C_{H_2} and C_{He} are empirically derived constants based upon measurements done by Karpowicz and Steffes (2011a), and all ideal pressures are in mbar.

The total absorption due to water vapor is written as

$$\alpha_{H_2O} = 4.342945 \times (\alpha_{lines} + \alpha_{continuum}) \quad (\text{dB/km}) \quad (22)$$

The factor 4.342945 is a conversion factor from km^{-1} to dB/km.

The necessary empirically derived constants are summarized in Table 11. These differ slightly from the constants derived in Karpowicz and Steffes (2011a). The biggest change is the removal of a second term present in the Karpowicz and Steffes (2011a) water vapor self-continuum term. The second term was added to provide additional opacity so as to provide a better fit to data taken at

Table 11
Empirically derived constants for the modified Karpowicz and Steffes (2011a,b) H_2O water vapor model.

C_w	3.1×10^{-7}	$km^{-1} \times (mbars \times GHz)^{-2}$
$x_{continuum}$	12	
C_{H_2}	$5.07722009423 \times 10^{-11}$	$km^{-1} \times (mbars \times GHz)^{-2}$
C_{He}	$1.03562010226 \times 10^{-10}$	$km^{-1} \times (mbars \times GHz)^{-2}$

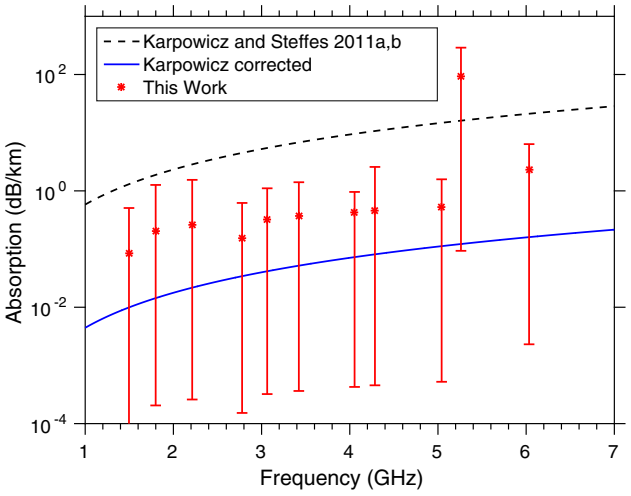

Fig. 7. Differential water vapor opacity data measured using the high-temperature centimeter-wavelength system at pressures of 4.734 bars and 3.612 bars at a temperature of 597 K.

525 K. However, subsequent re-calibration of the temperature data indicate that this term was not required (Karpowicz, private communication, 2012). Moreover, the additional term exhibited non-physical behavior at high temperatures. The empirically derived constant for water vapor (C_w) and the temperature exponent of the water vapor self-continuum ($x_{continuum}$) have been reset to allow use of the physically-based self-continuum expression from Rosenkranz (1998). Of the 929 measurement points used to develop the Karpowicz and Steffes (2011a); 2011b), this model revision fits 670 points within 2σ error bars. This is very similar to the 738 data points fit by the original (Karpowicz and Steffes, 2011a; 2011b) model.

The laboratory measurements of water vapor conducted at high temperature described in Section 3.2 are presented in Fig. 7. The result of these high temperature measurement of water vapor's microwave opacity are consistent with the modifications made to the Karpowicz and Steffes (2011a); 2011b) model.

4.4. Methane

Similar to water vapor's broadening of ammonia's absorption spectrum, the linewidth and coupling parameters are modified by adding the contribution of methane to Eqs. (13) and (14) as follows

$$\gamma_j = \gamma_{CH_4} P_{CH_4} \left(\frac{300}{T}\right)^{\Gamma_{CH_4}} + \gamma_{H_2} P_{H_2} \left(\frac{300}{T}\right)^{\Gamma_{H_2}} + \gamma_{He} P_{He} \left(\frac{300}{T}\right)^{\Gamma_{He}} + \gamma_{NH_3} \gamma_{(0,j)} P_{NH_3} \left(\frac{295}{T}\right)^{\Gamma_{NH_3}} \text{(GHz)} \quad (23)$$

$$\zeta_j = \zeta_{CH_4} P_{CH_4} \left(\frac{300}{T}\right)^{Z_{CH_4}} + \zeta_{H_2} P_{H_2} \left(\frac{300}{T}\right)^{Z_{H_2}} + \zeta_{He} P_{He} \left(\frac{300}{T}\right)^{Z_{He}} + \zeta_{NH_3} \gamma_{(0,j)} P_{NH_3} \left(\frac{295}{T}\right)^{Z_{NH_3}} \text{(GHz)} \quad (24)$$

Table 12
Constants for the new microwave opacity model of CH_4-broadened NH_3.

	i=CH_4	Units
γ_i	2.6406	(GHz/bar)
Γ_i	1.0	
ζ_i	0.9111	(GHz/bar)
Z_i	1.9200	

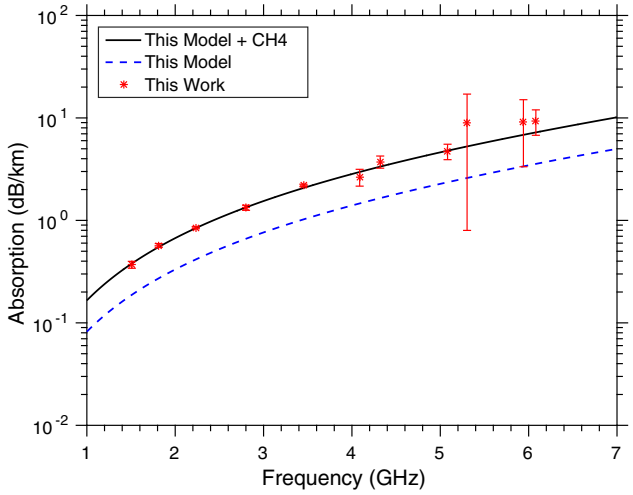

Fig. 8. Opacity data measured using the high-temperature centimeter-wavelength system for a mixture of NH_3 = 10.78%, CH_4 = 89.22% at a pressure of 1 bar and temperature of 329.4 K compared to the ammonia model presented in Section 4.1.1 and the ammonia model with methane added.

where for the inversion line j and constituent $i = CH_4$, H_2, He, NH_3, γ_i and ζ_i are constant scale terms, and Γ_i and Z_i represent the constant temperature dependences of the broadening and coupling of each of the gases, P_i are the ideal partial pressures in bar, and $\gamma_{(0,j)}$ are the self-broadening linewidths of the inversion transitions of ammonia in MHz/Torr.

The optimized free parameters for methane's scaling parameters and temperature dependences for both the linewidth and coupling parameters are derived through fitting the model to the laboratory results. The ammonia, hydrogen, and helium free parameters for the linewidth and coupling parameters are described previously in this work. Methane's line shape coefficients are displayed in Table 12.

This new model for the opacity of ammonia pressure-broadened by methane in the 5–20 cm wavelength range is fitted to opacity measurements at pressures up to 3 bars and a temperature range of 330 to 450 K.

In Figs. 8–10, the model for the opacity of ammonia which has been pressure-broadened by methane is plotted along with a subset of the opacity measurements taken in the laboratory. All 264 measurements taken in the 330–450 K temperature region at pressures of up to 3 bars (including either 100 mbar or 200 mbar of ammonia) conducted in this work were used to evaluate the performance of the model in the 1.5–6 GHz range. The error bars of each data point display the 2σ total uncertainties and uncertainty due to experimental conditions. The formalism accurately models 89.77% of all data points within the 2σ uncertainty.

5. Conclusion

Accurate laboratory measurements of the 5–20 cm-wavelength properties of ammonia in a high temperature environment have been conducted. These and previous laboratory measurements

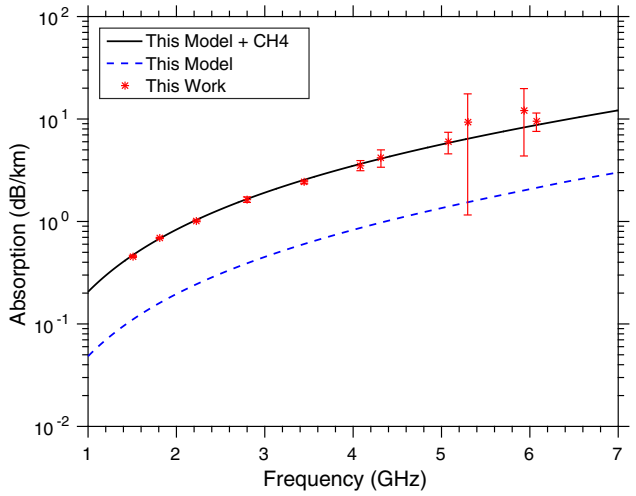

Fig. 9. Opacity data measured using the high-temperature centimeter-wavelength system for a mixture of NH_3 = 3.39%, CH_4 = 96.61% at a pressure of 2.992 bars and temperature of 375 K compared to the ammonia model presented in Section 4.1.1 and the ammonia model with methane added.

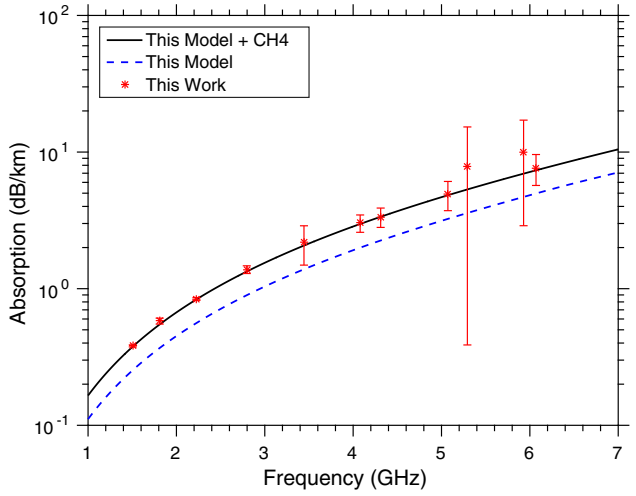

Fig. 10. Opacity data measured using the high-temperature centimeter-wavelength system for a mixture of NH_3 = 20.37%, CH_4 = 79.63% at a pressure of 1 bar and temperature of 449.8 K compared to the ammonia model presented in Section 4.1.1 and the ammonia model with methane added.

(Devaraj et al., 2014; 2011; Hanley et al., 2009) were used to develop the most physical, accurate, and consistent model of ammonia's opacity when pressure-broadened by hydrogen and helium. Weaknesses in previous ammonia models have been identified and reconciled in this new ammonia model.

Additionally, non-physical behaviors in the Karpowicz and Steffes (2011a); 2011b) centimeter-wavelength water vapor model have also been identified. Corrections have been implemented and have been verified by a high temperature differential laboratory measurement of water vapor's microwave opacity.

Finally, the influence of methane on ammonia's centimeter-wavelength absorption spectrum has been studied and modeled. While methane is a minor constituent in the atmospheres of Jupiter and Saturn (less than 0.5%), it has a major effect on the microwave opacity from ammonia in the atmosphere of Uranus and Neptune. Also of importance to both the Juno mission and to observations of other jovian planets, the additional measurement involving methane and hydrogen confirms the previous laboratory measurements made by Jenkins and Steffes (1988) indicating that methane is microwave-transparent at centimeter-wavelengths.

Acknowledgment

This work was supported by NASA Contract NNM06AA75C from the Marshall Space Flight Center supporting the Juno Mission Science team, under Subcontract 699054X from the Southwest Research Institute.

Appendix A. Measurement theory

The quality factor of a resonance is given by Mattaei and Jones (1980)

$$Q = \frac{2\pi f_0 \times \text{Energy Stored}}{\text{Average Power Loss}} \tag{A.1}$$

where f_0 is the resonant frequency. The Q of a resonance can be measured directly from f_0 by dividing it by its half-power bandwidth (HPBW).

$$Q = \frac{f_0}{HPBW} \tag{A.2}$$

The Q of a lossy gas (ϵ'/ϵ'') and its opacity are related by

$$\alpha \approx \frac{\epsilon''\pi}{\epsilon'\lambda} = \frac{1}{Q_{gas}}\frac{\pi}{\lambda} \tag{A.3}$$

where ϵ' and ϵ'' are the real and imaginary permittivity of the gas, λ is the wavelength in km, and α is the absoptivity of the gas in Nepers/km (1 Neper/km = 2 optical depths (km^{-1}) = 8.686 dB/km) (DeBoer and Steffes, 1994). Since Q is affected by more than just the gas under test, the Q of the gas-filled resonator is given by

$$\frac{1}{Q^m_{loaded}} = \frac{1}{Q_{gas}} + \frac{1}{Q_r} + \frac{1}{Q_{ext1}} + \frac{1}{Q_{ext2}} \tag{A.4}$$

where Q^m_{loaded} is the measured quality factor of a resonance in the presence of a test gas, Q_{gas} is the quality factor of the gas under test, Q_r is the quality factor of the evacuated resonator in the absence of coupling losses, and Q_{ext1} and Q_{ext2} are the external coupling losses. Since the resonator used is symmetric, we assume $Q_{ext1} = Q_{ext2}$. Coupling losses can be derived from the transmissivity $t = 10^{-S/10}$, where S is the measured insertion loss of the resonator in decibels (dB) at the frequency of a particular resonance using the following relationship (Mattaei and Jones, 1980)

$$t = \left[2\frac{Q^m}{Q_{ext}}\right]^2, \tag{A.5}$$

$$Q_{ext} = \frac{2Q^m}{\sqrt{t}} \tag{A.6}$$

Q_r is related to the measured Q at a vacuum by

$$\frac{1}{Q^m_{vac}} = \frac{1}{Q_r} + \frac{1}{Q_{ext1}} + \frac{1}{Q_{ext2}} \tag{A.7}$$

where Q^m_{vac} is the measured Q under vacuum conditions. Substituting Eq. (A.6) into Eqs. (A.4) and (A.7) gives

$$\frac{1}{Q_{gas}} = \frac{1-\sqrt{t_{loaded}}}{Q^m_{loaded}} - \frac{1-\sqrt{t_{vac}}}{Q^m_{vac}} \tag{A.8}$$

where t_{loaded} and t_{vac} are the transmissivity of the resonance taken in loaded and vacuum conditions, respectively. When gas is added to the resonator there is a shift in the center frequency corresponding to the refractive index of the test gas. Since the quality factor is reliant on the center frequency this will affect the comparison between the two measurements, even if the gas being tested is lossless. This effect is called dielectric loading (DeBoer and Steffes, 1994). This effect can be corrected by performing additional measurements of the quality factor with a lossless gas present. Adding the lossless gas shifts the center frequency of the

resonances, and by adding more or less gas, the center frequency can be adjusted to be exactly the same as the lossy gas. These measurements are used in place of the vacuum measurements in Eq. (A.8) and by converting Nepers/km to dB/km Eq. (A.3) becomes

$$\alpha = 8.686\frac{\pi}{\lambda}\left(\frac{1-\sqrt{t_{loaded}}}{Q^m_{loaded}} - \frac{1-\sqrt{t_{matched}}}{Q^m_{matched}}\right)\text{dB/km} \quad \text{(A.9)}$$

An important note is that an absorption coefficient of 1 Nepers/km = 2 optical depths per km (or km^{-1}) = 8.686 dB/km. The first notation is used in electrical engineering, the second is the usual form in physics and astronomy, and the third is the common (logarithmic) form. The third form is often used in order to avoid a possible factor-of-two ambiguity.

References

Atreya, S., Mahaffy, P., Niemann, H., et al., 2003. Composition and origin of the atmosphere of jupiteran update, and implications for the extrasolar giant planets. Planet. Space Sci. 51 (2), 105–112.

Ben-Reuven, A., 1966. Impact broadening of microwave spectra. Phys. Rev. 145, 7–22. http://link.aps.org/doi/10.1103/PhysRev.145.7.

Berge, G., Gulkis, S., 1976. Earth-based Observations of Jupiter: Millimeter to Meter Wavelengths. Technical Report. Owens Valley Radio Observatory, Pasadena, California, USA.

Byrd, R.H., Lu, P., Nocedal, J., et al., 1995. A limited memory algorithm for bound constrained optimization. SIAM J. Sci. Comput. 16 (5), 1190–1208.

DeBoer, D.R., Steffes, P.G., 1994. Laboratory measurements of the microwave properties of H2S under simulated jovian conditions with an application to neptune. Icarus 109 (2), 352–366. http://www.sciencedirect.com/science/article/pii/S0019103584710992.

Devaraj, K., Steffes, P.G., Duong, D., 2014. The centimeter-wavelength opacity of ammonia under deep jovian conditions. Icarus 241, 165–179. http://www.sciencedirect.com/science/article/pii/S0019103514003285.

Devaraj, K., Steffes, P.G., Karpowicz, B.M., 2011. Reconciling the centimeter- and millimeter-wavelength ammonia absorption spectra under jovian conditions: Extensive millimeter-wavelength measurements and a consistent model. Icarus 212 (1), 224–235. http://www.sciencedirect.com/science/article/pii/S0019103510004677.

Gross, E.P., 1955. Shape of collision-broadened spectral lines. Phys. Rev. 97, 395–403. http://link.aps.org/doi/10.1103/PhysRev.97.395.

Hanley, T.R., Steffes, P.G., 2007. A high-sensitivity laboratory system for measuring the microwave properties of gases under simulated conditions for planetary atmospheres. Radio Sci. 42 (6). http://dx.doi.org/10.1029/2007RS003693.

Hanley, T.R., Steffes, P.G., Karpowicz, B.M., 2009. A new model of the hydrogen and helium-broadened microwave opacity of ammonia based on extensive laboratory measurements. Icarus 202 (1), 316–335. http://www.sciencedirect.com/science/article/pii/S0019103509000451.

Janssen, M., Hofstadter, M., Gulkis, S., et al., 2005. Microwave remote sensing of Jupiter's atmosphere from an orbiting spacecraft. Icarus 173 (2), 447–453.

Janssen, M., Ingersoll, A., Allison, M., et al., 2013. Saturns thermal emission at 2.2-cm wavelength as imaged by the cassini radar radiometer. Icarus 226 (1), 522–535.

Janssen, M.A., 1993. In: Janssen, M.A. (Ed.), Atmospheric Remote Sensing By Microwave Radiometry, Vol. 1. Wiley, New York, NY. LC# QC871. J26 1993. ISBN# 0471628913.

Jenkins, J.M., Steffes, P.G., 1988. Constraints on the microwave opacity of gaseous methane and water vapor in the jovian atmosphere. Icarus 76 (2), 378–382.

Joiner, J., Steffes, P.G., 1991. Modeling of jupiter's millimeter wave emission utilizing laboratory measurements of ammonia (nh3) opacity. J. Geophys. Res. 96 (E2), 17463–17470.

Karpowicz, B.M., Steffes, P.G., 2011a. In search of water vapor on jupiter: Laboratory measurements of the microwave properties of water vapor under simulated jovian conditions. Icarus 212 (1), 210–223. http://www.sciencedirect.com/science/article/pii/S0019103510004549.

Karpowicz, B.M., Steffes, P.G., 2011b. Corrigendum to in search of water vapor on jupiter: Laboratory measurements of the microwave properties of water vapor under simulated jovian conditions [Icarus 212 (2011) 210223]. Icarus 214 (2), 783. http://www.sciencedirect.com/science/article/pii/S0019103511002119.

Matousek, S., 2005. The Juno New Frontiers Mission. California Institute of Technology. Technical Report IAC-05-A3.2.A.04

Mattaei, G.L., Jones, E., 1980. Microwave Filters, Impedance Matching Networks and Coupling Structures. McGraw-Hill, New York.

de Pater, I., Butler, B., Green, D., et al., 2003. Jupiters radio spectrum from 74 MHz up to 8 GHz. Icarus 163 (2), 434–448.

de Pater, I., DeBoer, D., Marley, M., et al., 2005. Retrieval of water in jupiter's deep atmosphere using microwave spectra of its brightness temperature. Icarus 173 (2), 425–438.

de Pater, I., Lissauer, J.J., 2001. Planetary Sciences.. Cambridge University Press.

de Pater, I., Mitchell, D.L., 1993. Radio observations of the planets: The importance of laboratory measurements. J. Geophys. Res. 98 (E3), 5471–5490.

Pickett, H., Poynter, R., Cohen, E., et al., 1998. Submillimeter, millimeter, and microwave spectral line catalog. J. Quant. Spectrosc. Radiat. Transf. 60 (5), 883–890. http://www.sciencedirect.com/science/article/pii/S0022407398000910.

Pingree, P., Janssen, M., Oswald, J., et al., 2008. Microwave radiometers from 0.6 to 22 GHz for juno, a polar orbiter around jupiter. In: Proceedings of 2008 IEEE Aerospace Conference. IEEE, pp. 1–15.

Poynter, R.L., Kakar, R.K., 1975. The microwave frequencies, line parameters, and spectral constants for NH3-14. Astrophys. J. Suppl. 29, 87–96. http://dx.doi.org/10.1086/190334.

Rosenkranz, P.W., 1998. Water vapor microwave continuum absorption: A comparison of measurements and models. Radio Sci. 33 (4), 919–928.

Townes, C.H., Schawlow, A.L., 1975. Microwave Spectroscopy. Dover Publications.

Yu, S., Drouin, B., Pearson, J., 2010a. Species tag: 17002 version 5.URL http://spec.jpl.nasa.gov/ftp/pub/catalog/doc/d017002.pdf

Yu, S., Drouin, B., Pearson, J., 2010b. Species tag: 17004 version 5.URL http://spec.jpl.nasa.gov/ftp/pub/catalog/doc/d017004.pdf

Yu, S., Pearson, J.C., Drouin, B.J., et al., 2010c. Submillimeter-wave and far-infrared spectroscopy of high-j transitions of the ground and $\nu 2 = 1$ states of ammonia. J. Chemi. Phys. 133 (17), 174317.